Dependence of Heat and Particle Transport on the Ratio of the Ion and Electron Temperatures

C. C. Petty,[1] M. R. Wade,[2] J. E. Kinsey,[3] R. J. Groebner,[1] T. C. Luce,[1] and G. M. Staebler[1]
[1]*General Atomics, San Diego, California 92186-5608*
[2]*Oak Ridge National Laboratory, Oak Ridge, Tennessee 37831-2009*
[3]*Lehigh University, Bethlehem, Pennsylvania 18015*
(Received 14 May 1999)

Experiments in high confinement (H-mode) plasmas on the DIII-D tokamak show that the heat and particle transport are sensitive to the ratio of the ion and electron temperatures. Increasing the ion-to-electron temperature ratio decreases the electron and ion heat transport and the particle transport regardless of which temperature is being varied. A likely explanation of these results is the dependence of the ion-temperature-gradient instability on the ratio of the ion and electron temperatures.

PACS numbers: 52.55.Fa, 52.25.Fi

Plasmas of interest to magnetic confinement fusion can be thought of as comprising separate ion and electron fluids, each fluid with its own density and temperature. The ion and electron densities (n_i and n_e) are related by the overriding tendency of the plasma to remain electrically neutral, but the ion and electron temperatures (T_i and T_e) can be quite different since the thermal equilibration time between the two fluids may be longer than the energy confinement time of the plasma. A large body of previous work has shown that cross-magnetic-field diffusion of heat and particles (referred to as transport) is significantly reduced in plasmas with $T_i \gg T_e$. Nearly all of the best confinement modes on tokamaks occur in plasmas with T_i more than twice T_e: the "hot ion" H mode (high confinement) [1] and VH mode (very high confinement) [2], the "supershot" [3], and the negative magnetic shear regime [4,5]. However, T_i and T_e are expected to be nearly equal in future ignition devices owing to the longer confinement times and strong electron heating from the fusion products. Therefore, if transport has a strong dependence on the ratio of the ion and electron temperatures, then projecting the favorable transport results from hot ion mode plasmas to future ignition devices may lead to too optimistic predictions for confinement.

The experiments reported in this Letter are the first in which the ratio of the ion and electron temperatures is systematically varied to determine the effect on heat and particle transport. These experiments in ELMing (edge localized mode) H-mode plasmas are in a regime relevant to future ignition devices, with nearly equal ion and electron temperatures and T_i profiles close to marginal stability for the ion-temperature-gradient (ITG) mode. Three different T_i/T_e scans have been done, each of which addresses a specific question. First, a T_e scan at fixed T_i is performed to examine whether the ion heat transport is influenced by the electrons. Second, the converse, a T_i scan at fixed T_e shows how the electron heat transport is affected by the ions. Third, the ratio of T_i/T_e is varied at fixed β (the ratio of the plasma and magnetic field pressures) to determine if heat transport is dependent upon how the plasma pressure is divided between the electron and ion fluids. The helium particle transport is also measured for several of the T_i/T_e scans. For all of these experiments, the plasma density, current, and magnetic field strength are held fixed.

These experiments are done on the DIII-D tokamak [6], parameters for which are major radius $R = 1.68$ m, minor radius $a = 0.61$ m, elongation $\kappa = 1.8$, plasma current $I = 1.45$ MA, and magnetic field strength $B = 2.05$ T. Three different forms of auxiliary heating are used to control T_i and T_e in these experiments. The ions are heated by up to 4.9 MW of deuterium neutral beam injection (NBI); a small portion of this NBI power is also absorbed by the electrons. The electron temperature is increased further using up to 2.5 MW of combined electron cyclotron heating (ECH) and fast wave direct electron heating. The n_e and T_e profiles are measured by Thomson scattering, CO_2 laser interferometers, and electron cyclotron emission. The T_i and effective ion charge (Z_{eff}) profiles are determined from charge exchange recombination emission of carbon impurities.

In the first experiment, the electron temperature is varied at fixed ion temperature and density, as seen in Fig. 1,

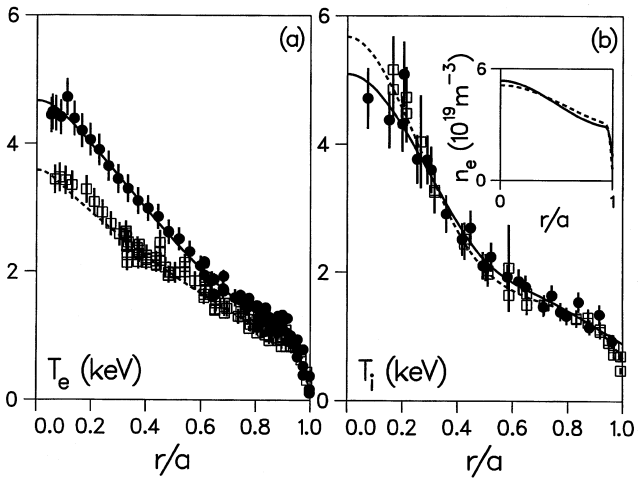

FIG. 1. (a) Electron temperature and (b) ion temperature profiles for the T_e scan at fixed T_i given in column (a) of Table I. The electron density profiles are also shown in (b).

TABLE I. Global parameters for three temperature scans at fixed B and I: (a) T_e scan at fixed T_i, (b) T_i scan at fixed T_e, and (c) T_i/T_e scan at fixed β.

	(a)		(b)		(c)	
Parameter	High T_e	Low T_e	High T_i	Low T_i	High T_i/T_e	Low T_i/T_e
$\langle n_e \rangle$ (10^{19} m^{-3})	3.6	3.7	4.0	3.9	3.6	3.7
$\langle Z_{\text{eff}} \rangle$	2.4	2.5	2.2	2.5	2.3	2.4
β_N [%/(MA/mT)]	1.11	1.00	1.39	1.09	1.27	1.25
P_i (MW)	2.7	2.0	3.0	2.1	2.9	2.8
P_e (MW)	4.1	1.8	1.8	3.8	1.7	3.8
τ_E (s)	0.089	0.148	0.161	0.104	0.154	0.105
τ_m (s)	0.076	0.129	0.118	0.106	0.100	0.074

and shows that confinement decreases with increasing T_e. The electron temperature is scanned by 26% in this experiment using ECH and fast wave heating while the NBI power is also increased to keep T_i fixed. The heating powers absorbed by the ions and electrons (P_i and P_e) are shown in column (a) of Table I along with the other global parameters. The data in Table I do not include fast particle contributions to the normalized beta [$\beta_N = \beta/(I/aB)$] and the energy confinement time (τ_E). Table I shows that the volume averaged $\langle n_e \rangle$ and $\langle Z_{\text{eff}} \rangle$ are held fixed to within 3% during the T_e scan, with the thermal energy confinement time scaling like $\tau_E \propto \langle T_e \rangle^{-2.2\pm0.2}$.

The thermal diffusivities (χ) for these discharges are determined from a radial power balance analysis, $1.5\partial(nT)/\partial t + \nabla \cdot (\mathbf{q} + 2.5\Gamma T) = Q$, where q is the heat flux, Γ is the particle flux, and the heat sources and sinks are combined into Q. The transport calculations are carried out using the ONETWO code [7], which uses the measured n_e, T_e, T_i, Z_{eff}, and P_{rad} profiles along with the magnetic geometry. The heat flux is assumed to be purely diffusive in this analysis, $q = -n\chi\nabla T$. The helium particle transport is determined by analyzing the evolution of the helium density profile shortly after a helium gas puff [8].

The transport analysis shows that the ion thermal diffusivity increases with increasing T_e at fixed T_i, demonstrating that the ion transport is not dependent solely upon the ion parameters but is also influenced by the electrons. Figure 2 shows the change in the electron and ion thermal diffusivities as a function of normalized radius (r/a) between the high-T_e and low-T_e cases of Fig. 1. The internal disruption, or sawtooth instability, is suppressed in these plasmas using NBI during the current ramp to broaden the current profile and keep the central safety factor above unity. Figure 2 shows that the ion thermal diffusivity increases with increasing electron temperature like $\chi_i \propto T_e^4$ for these plasmas; this strong dependence indicates that the ion heat transport is sensitive to T_e in this regime. This sensitivity is likely due to the destabilization of the ITG mode, as discussed later in this Letter. The electron thermal diffusivity also tends to increase for higher T_e but in a more complicated manner than the ions, perhaps indicating that χ_e depends upon both T_e and ∇T_e. Figure 2 also shows that the helium particle transport increases with increasing T_e by an amount that is between the χ_i and χ_e dependences.

In the second experiment, the ion temperature is varied at nearly constant electron temperature and density, as shown in Fig. 3, and it is found that confinement *increases* with increasing T_i. This is the opposite trend as found for the T_e scan. The ion temperature is varied by 24% by increasing the NBI power and decreasing the ECH and fast wave power at fixed density, as shown in column (b) of Table I. Since the thermal energy confinement time in this case increases with increasing ion temperature like $\tau_E \propto \langle T_i \rangle^{2.0\pm0.2}$, a higher value of β is achieved for the plasma with higher T_i/T_e despite less total heating power. A local transport analysis confirms these results. In Fig. 4, the electron thermal diffusivity is seen to decrease with increasing ion temperature approximately like $\chi_e \propto T_i^{-4}$, demonstrating that the electron heat transport is sensitive to T_i in this regime. The ion thermal diffusivity also decreases with increasing T_i in Fig. 4, although this dependence is more complicated to interpret since both T_i

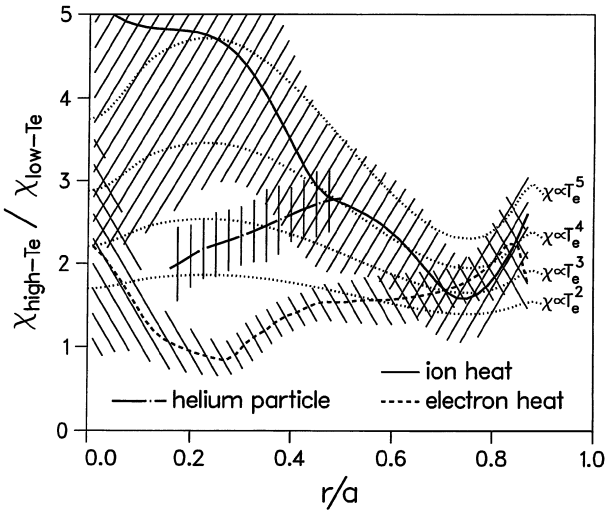

FIG. 2. Ratio of electron and ion thermal diffusivities and helium particle diffusivity for the T_e scan at fixed T_i shown in Fig. 1. The lined shading indicates the standard deviation of the random error.

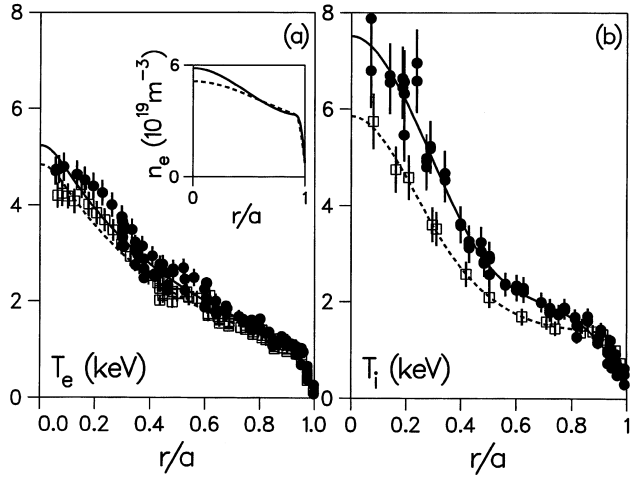

FIG. 3. (a) Electron temperature and (b) ion temperature profiles for the T_i scan at fixed T_e given in column (b) of Table I. The electron density profiles are also shown in (a).

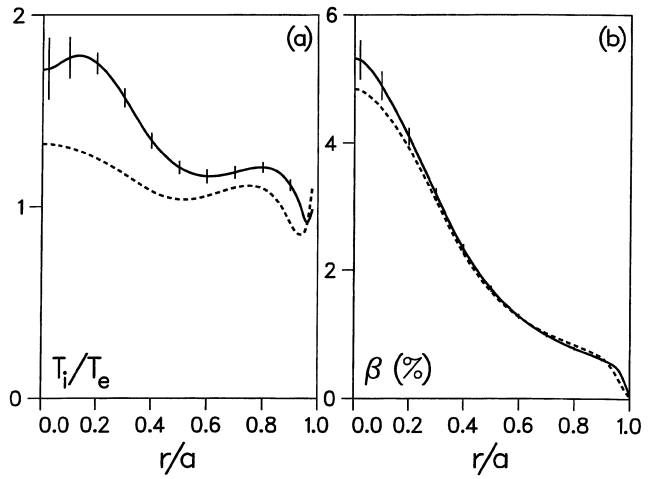

FIG. 5. (a) Ratio of ion and electron temperatures and (b) thermal beta for the T_i/T_e scan at fixed β given in column (c) of Table I.

and ∇T_i are varying. The positive reinforcement between χ_i and T_i likely contributes to forming the favorable hot ion mode of confinement [1–5].

In the third experiment, the ratio of the ion and electron temperatures is varied at fixed β, as seen in Fig. 5, and shows that transport is dependent upon how the plasma stored energy is divided between the electron and ion fluids. For a 20% scan in T_i/T_e, column (c) of Table I shows that the thermal energy confinement time increases with increasing ion-to-electron temperature ratio like $\tau_E \propto (\langle T_i\rangle/\langle T_e\rangle)^{2.1\pm0.2}$, which agrees with the results from the first two experiments in Table I. The local heat transport dependence on T_i/T_e, shown in Fig. 6, is also consistent with the transport dependences on T_e and T_i shown in Figs. 2 and 4, with both the electron and ion thermal diffusivities decreasing for higher $\langle T_i\rangle/\langle T_e\rangle$. (Since T_e, ∇T_e, T_i, and ∇T_i are all varying in this case, only the scalings with the volume averaged temperatures are indicated in Fig. 6 for simplicity.) Figure 6 also shows that the helium particle diffusivity decreases with increasing $\langle T_i\rangle/\langle T_e\rangle$ by an amount that is similar to the electron thermal diffusivity.

The momentum confinement times (τ_m) given in Table I also increase with increasing T_i/T_e, similar to the energy confinement results. A regression analysis of this dependence over all discharges shows that $\tau_m \propto \langle T_i\rangle/\langle T_e\rangle^3$. Thus, the plasma rotation slows down with the application of ECH and fast wave heating, which in turn causes the measured $E \times B$ shearing rate to vary by as much as 30% in the outer half of the plasma. (We note that the computed $E \times B$ shearing rate obtained

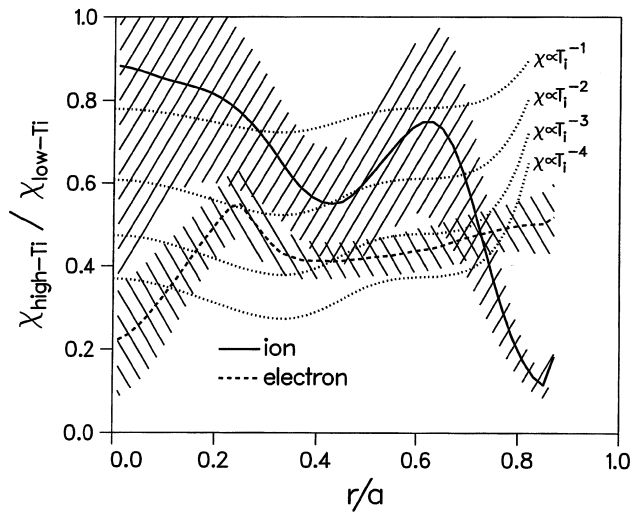

FIG. 4. Ratio of electron and ion thermal diffusivities for the T_i scan at fixed T_e shown in Fig. 3.

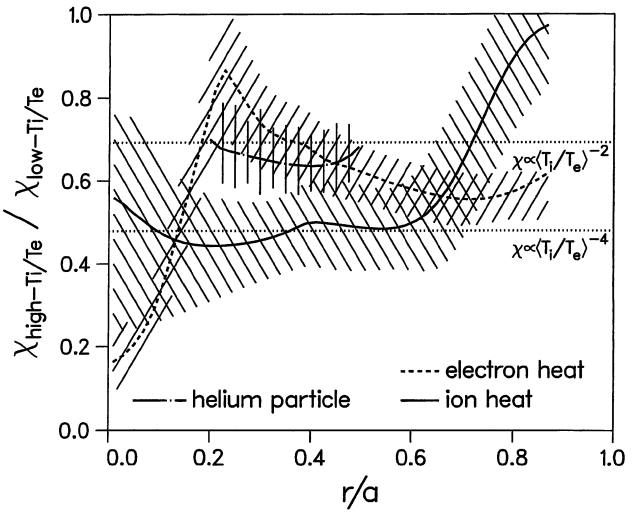

FIG. 6. Ratio of electron and ion thermal diffusivities and helium particle diffusivity for the T_i/T_e scan at fixed β shown in Fig. 5.

from the experimental toroidal velocity profile and the calculated poloidal velocity profile from neoclassical theory differs from the measured $E \times B$ shearing rate by as much as a factor of 2 and exhibits the wrong radial shape.) Since $E \times B$ shear can reduce the heat and particle transport by connecting unstable modes to stable modes [9], the sensitivity of the transport results to variations in the $E \times B$ shear warrants examination. Simulations using the gyro-Landau-fluid GLF23 drift wave transport model [10] in the MLT code [11] show that while the $E \times B$ shear is acting to reduce the overall level of transport, the differences in the $E \times B$ shear within the T_i/T_e scan have a negligible effect on the predicted temperature profiles. Differences in the n_e, n_i, and Z_{eff} within the T_i/T_e scan are also predicted to have less than a 10% cumulative effect on the transport.

The sensitivity of the heat and particle transport to the ratio of the ion and electron temperatures is likely due to the destabilization of the ITG mode (the electron temperature gradient mode is predicted to be stable). Modeling of these H-mode plasmas using the GLF23 transport model shows that the measured T_i profile in this regime is close to marginal stability for the ITG mode. The ITG mode is predicted to be unstable when the density scale length divided by the ion temperature scale length (L_n/L_{T_i}) exceeds a threshold that can be characterized by a critical value of L_{T_i}/R in the flat density limit [12,13]. Since the critical ion temperature gradient for the onset of this mode increases with increasing T_i/T_e, an increase in T_e at fixed T_i will increase the ITG driven heat and particle transport. The sensitivity of the measured heat and particle transport to T_i/T_e can be explained by the large incremental diffusivity of the ITG mode, which tends to pin the ion temperature gradient to the critical value. Figure 7(a) shows the scaling of the predicted thermal diffusivities for the T_e scan at fixed T_i (Figs. 1 and 2) using the GLF23 model. In the simulation, the measured density and rotation profiles are utilized and the T_i and T_e profiles are calculated using the radial heat fluxes obtained from a power balance analysis. The GLF23 model predicts a similar sensitivity of transport to T_i/T_e as is observed experimentally, with the theoretical thermal diffusivities in Fig. 7(a) increasing by nearly the same amount as found in the experiment; the particle diffusivity has a similar T_i/T_e dependence. The strong T_i/T_e dependence of transport in the GLF23 model for the T_e scan at fixed T_i is better seen in Fig. 7(b), which shows that $\chi_i \propto (T_i/T_e)^{-3.0}$ and $\chi_e \propto (T_i/T_e)^{-2.2}$ around the experimental point.

In conclusion, experiments in ELMing H-mode plasmas on the DIII-D tokamak have measured the dependence of cross-magnetic-field transport on the ratio of the ion and electron temperatures and show a strong temperature coupling effect between the ion and electron fluids. The electron and ion thermal diffusivities, the helium particle diffusivity, and the momentum transport all decrease with increasing T_i/T_e, regardless of which temperature is being varied. The sensitivity of confinement to changes in the ion-to-electron temperature ratio, $\tau_E \propto (T_i/T_e)^2$, is likely explained by the destabilization of the ITG mode near threshold given the T_i/T_e dependence of the critical ion temperature gradient.

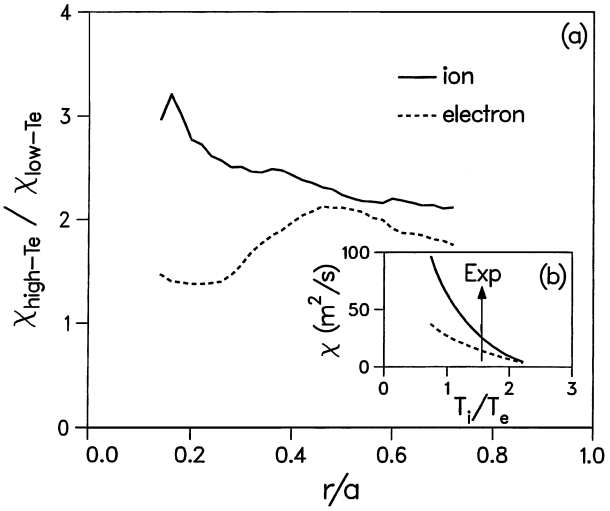

FIG. 7. (a) Predicted ratio of electron and ion thermal diffusivities and (b) predicted dependence of χ_i and χ_e on the ion-to-electron temperature ratio at $r/a = 0.2$ from the GLF23 model for the T_e scan at fixed T_i shown in Fig. 2. The location of the experimental point is also indicated in (b).

The authors thank J. S. deGrassie, E. A. Lazarus, J. Lohr, F. W. Baity, and R. I. Pinsker for operating the tokamak and radiofrequency heating systems for these experiments. This work is supported by the U.S. Department of Energy under Contracts No. DE-AC03-99ER54463 and No. DE-AC05-96OR22464.

[1] K. H. Burrell *et al.*, in *Plasma Physics and Controlled Nuclear Fusion Research, Washington, DC, 1990* (IAEA, Vienna, 1991), Vol. 1, p. 123.
[2] G. L. Jackson *et al.*, Phys. Rev. Lett. **67**, 3098 (1991).
[3] J. D. Strachan *et al.*, Phys. Rev. Lett. **58**, 1004 (1987).
[4] F. M. Levinton *et al.*, Phys. Rev. Lett. **75**, 4417 (1995).
[5] E. J. Strait *et al.*, Phys. Rev. Lett. **75**, 4421 (1995).
[6] J. L. Luxon and L. G. Davis, Fusion Technol. **8**, 441 (1985).
[7] H. St. John *et al.*, in *Plasma Physics and Controlled Nuclear Fusion Research, Seville, 1994* (IAEA, Vienna, 1995), Vol. 3, p. 603.
[8] M. R. Wade *et al.*, Phys. Plasmas **2**, 2357 (1995).
[9] R. E. Waltz, R. L. Dewar, and X. Garbet, Phys. Plasmas **5**, 1784 (1998).
[10] R. E. Waltz *et al.*, Phys. Plasmas **4**, 2482 (1997).
[11] J. A. Konings and R. E. Waltz, Nucl. Fusion **37**, 863 (1997).
[12] W. M. Tang, G. Rewoldt, and L. Chen, Phys. Fluids **29**, 3715 (1986).
[13] R. R. Dominguez and R. E. Waltz, Phys. Fluids **31**, 3147 (1988).